The time-varying electron energy distribution function in the plume of a Hall thruster

2014 Plasma Sources Sci. Technol. 23 065001

(http://iopscience.iop.org/0963-0252/23/6/065001)

IOP Publishing Plasma Sources Science and Technology

Plasma Sources Sci. Technol. **23** (2014) 065001 (8pp) doi:10.1088/0963-0252/23/6/065001

The time-varying electron energy distribution function in the plume of a Hall thruster

K Dannenmayer[1], S Mazouffre[1], P Kudrna[2] and M Tichý[2]

[1] Institut de Combustion, Aérothermique, Réactivité et Environnement, CNRS, Orléans, France
[2] Charles University, Faculty of Mathematics and Physics, Prague, Czech Republic

E-mail: stephane.mazouffre@cnrs-orleans.fr

Received 11 March 2014, revised 2 June 2014
Accepted for publication 23 June 2014
Published 7 August 2014

Abstract

Time-resolved Langmuir probe measurements have been performed in the plume of the 1.5 kW class PPS®1350-ML Hall thruster. The time-dependent electron energy distribution function (EEDF) has been inferred from the probe current–voltage characteristic curves obtained after active stabilization of the discharge. The distribution function changes in the course of time at the breathing oscillation frequency (13.8 kHz). The EEDF is Maxwellian with a depleted tail above the xenon ionization energy whatever the location and the time. The electron density and temperature computed from the EEDF also oscillate at the breathing mode frequency. Experimental outcomes indicate the existence of a low-frequency plasma wave that propagates axially. The wave front speed (2700 m s^{-1}) was found to be compatible with the ion acoustic speed (2300 m s^{-1}).

Keywords: electric propulsion, Langmuir probe, EEDF

(Some figures may appear in colour only in the online journal)

1. Introduction

Hall thrusters are efficient plasma accelerators dedicated to space applications [1–3]. Their configuration is based on crossed magnetic and electric fields to ionize and accelerate a propellant gas. Hall thrusters are currently employed for geostationary communication satellites orbit correction and station keeping. The next generation of Hall thrusters will be devoted to maneuvers and missions that require a higher thrust level like satellite orbit transfer and solar system exploration.

A Hall thruster is a magnetized low-pressure dc discharge maintained between an external cathode and an anode [4, 5]. The anode, which often serves as a gas injector, is located at the upstream end of a coaxial annular dielectric channel that confines the discharge. Xenon is used as the propellant gas for its specific properties in terms of atomic mass and low ionization energy. A set of solenoids or permanent magnets provides a radially directed magnetic field, the strength of which is maximum in the vicinity of the channel exhaust. The magnetic field is chosen strong enough to make the electron Larmor radius much smaller than the thruster discharge chamber sizes, but weak enough not to affect ion trajectories. The electric potential drop is mostly concentrated in the final section of the channel owing to the high electron resistivity. The corresponding local axial electric field drives a large azimuthal electron drift—the Hall current—which is responsible for the efficient ionization of the gas. The electric field also accelerates ions out of the channel, which generates thrust. The ion beam is neutralized by a fraction of the electrons emitted from the cathode.

The magnetized plasma of a Hall thruster displays numerous types of oscillations, which encompass many kind of physical phenomena, each of them with its own length and time scale [6, 7]. Plasma oscillations, of which the spectrum stretches from the kHz to the GHz frequency domain, play a major role in ionization, particle diffusion and acceleration. Longitudinal oscillations in the direction of the electric field in the 10–30 kHz band, however, largely dominate the power spectrum. These oscillations, which originate in a prey–predator-type ionization cycle inside the thruster channel, are referred to as ‘breathing oscillations’ in the literature [8, 9]. Time-resolved measurements of plasma parameters

at the breathing mode time scale are therefore necessary to capture fine details about physical mechanisms that govern the properties and the performance of the device. Experimental data about discharge dynamics is also critical for the validation of models and associated computer simulations that are essential tools for the design of optimized thrusters. In recent years, time-resolved measurements of the plasma potential V_p, the electron temperature T_e and the electron density n_e have been performed near the channel exhaust and far in the plume of various Hall thrusters by Smith [10], Lobbia [11] and Dannenmayer [12] using Langmuir as well as emissive probes. All of these authors found oscillations of the parameters at the breathing frequency. Changes in time of T_e and V_p are pronounced and correlated. The electron density also varies during one period. In this contribution, we examine the time-dependent electron energy distribution function (EEDF) in the plume of a 1.5 kW-class Hall thruster. The EEDF allows us to compute n_e and T_e without the assumption of a Maxwellian distribution. As well as this, it gives information about the thermodynamic state of the medium and collision processes at stake. The EEDF(t) is captured by means of a cylindrical Langmuir probe. The breathing oscillation is stabilized by applying a sinusoidal voltage modulation on a floating electrode in the vicinity of the cathode. This specific approach warrants a high signal-to-noise ratio as temporal coherence between cycles is enhanced and the discharge frequency content does not change substantially in time [12].

2. Experimental arrangement

2.1. Hall thruster

Experiments were carried out in the downstream plume of the 1.5 kW class PPS®1350-ML Hall. The PPS®1350-ML is the laboratory model of the PPS®1350 thruster developed by Snecma that successfully propelled the SMART-1 space probe during its journey to the Moon [13]. The thruster was fired in the PIVOINE-2g test-bench. The thruster was equipped with BN-SiO_2 channel walls. The magnetic field stayed unchanged with a 4.5 A coil current. The applied voltage U_d was kept fixed at (250 ± 3) V. The anode xenon gas mass flow rate and the cathode mass flow rate were (3.0 ± 0.1) mg s^{-1} and (0.40 ± 0.01) mg s^{-1}, respectively. The discharge current, measured on the anode line with a calibrated Tektronix TCP202 dc coupled current-probe (dc to 50 MHz bandwidth), was (2.32 ± 0.02) A, meaning the input electrical power reached (580 ± 12) W. Operating conditions were chosen to avoid damaging the amplifier used to stabilize the discharge. The cathode-to-ground potential was −17 V. The background pressure inside the vacuum chamber was maintained at (2 ± 1) × 10^{-5} mbar-Xe during operation.

The layout of the experimental setup is shown in figure 1. The thruster was mounted on a moveable arm, which allowed a displacement along the thrust axis (in the x-direction). The electrostatic probe was mounted on a second arm, the so-called diagnostics arm, that moves perpendicular to the thrust axis

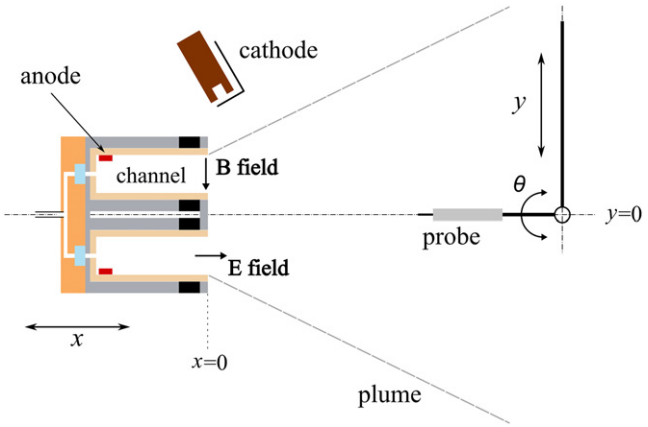

Figure 1. Layout of the experimental setup with the coordinate system (not to scale).

(in the y-direction). A rotation stage at the end of the diagnostics arm allowed us to set the probe angle in such a way that the probes always pointed toward the thruster center. A combination of the displacements of the probes in the y- and θ-direction, together with the possibility of moving the thruster along its axis, permits the cartography of the far-field plume in polar coordinates [14]. The position $x = 0$ refers to the thruster channel exit plane and the position $y = 0$ indicates the thruster axis—see figure 1.

2.2. Langmuir probes and the measurement procedure

A single cylindrical Langmuir probe was used to acquire the time-varying current–voltage characteristic curve necessary for the determination of the time evolution of the EEDF. The Langmuir probe was made of a 0.38 mm diameter tungsten wire. The non-collecting part of the wire was insulated from the plasma by a 100 mm long and 2 mm diameter alumina tube. The length of the collecting part was 5 mm. The voltage sweep and the resulting probe current measurement were performed using the ALP System™ manufactured by Impedans. In order to measure the time-dependent I–V characteristic, the probe current was recorded over one oscillation period for a fixed bias voltage. By repeating such measurements for a broad range of probe voltages, one obtains a two-dimensional matrix of probe currents with time and voltage as independent variables. The time-dependent probe characteristics can be recovered from this matrix. In this work, the time resolution was set to 0.5 μs and the probe bias voltage step was 0.2 V. The time series corresponded to an ensemble average over 1000 oscillation cycles. Notice that the time resolution warranted unaffected measurements. Firstly, the sampling frequency of the ALP unit was 25 ns and the current measurement was performed with a low impedance. The RC time constant of the system was therefore below 0.1 μs. Secondly, the temporal response of the probe was given by the ion plasma frequency. Under our conditions ($n_e = 3 \times 10^{16}$ m^{-3}), the frequency was around 3 MHz.

In order to guarantee repeatable measurement conditions, the thruster has to be maintained in a quasiperiodic oscillation regime. This was achieved by applying a sinusoidal potential

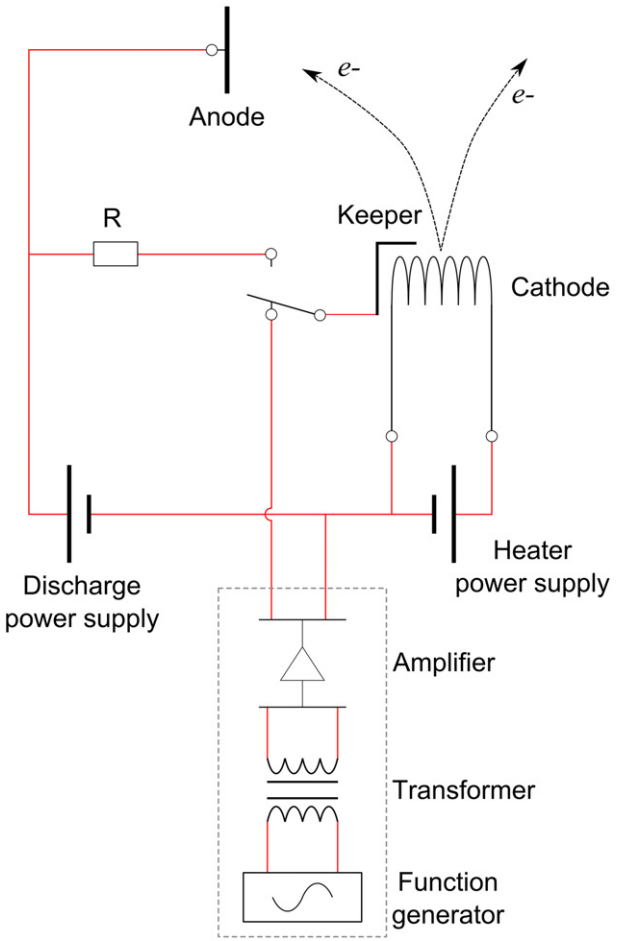

Figure 2. Schematic view of the electrical circuit for the keeper electrode voltage modulation. The two power supplies are floating. The keeper load resistor R is 1 kΩ.

modulation between a floating electrode placed in the plasma, here the cathode keeper, and the negative pole of the cathode heating circuit. A schematic view of the electrical circuitry is shown in figure 2. A detailed description of this method can be found in [12]. It has already been successfully applied to investigate the time evolution of electron parameters [12] and ion velocity [15] in the plasma of a low-power Hall thruster. The influence of the voltage modulation on the discharge current is shown in figure 3. The thruster was maintained in a quasiperiodic oscillation regime with a 200 V peak-to-peak 13.8 kHz modulation applied to the keeper. This frequency corresponds to the breathing mode frequency under our operating condition. The associated period is 71 μs. A 0.2 A current flowed through the keeper, which means about 40 W of power was supplied to the discharge. Notice the time-averaged value of microscopic and macroscopic quantities is not affected by the modulation [12, 15].

3. The electron energy distribution function

For an isotropic plasma, and in the case of a convex small probe, the EEDF $f(\varepsilon)$ can be obtained from the second derivative of the probe I–V characteristic with respect to the applied

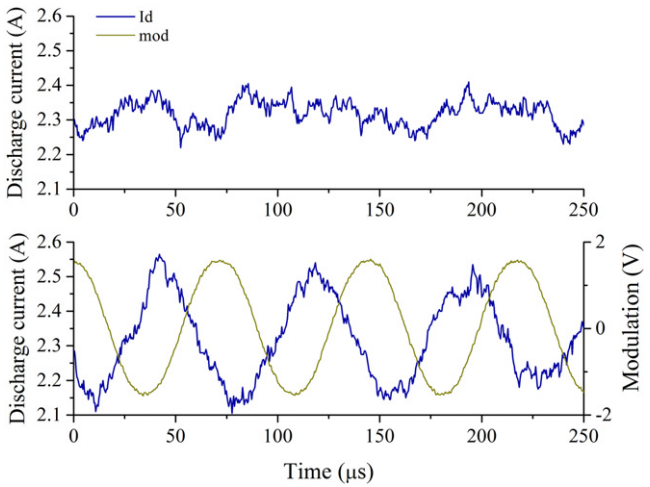

Figure 3. The time evolution of the discharge current without (top) and with (bottom) voltage modulation at 13.8 kHz (71 μs) applied between the cathode and the keeper electrode. The modulation waveform is shown here before amplification. The mean discharge current was equal to 2.32 A in the two cases.

potential [16, 17]. The so-called Druyvesteyn relation reads:

$$\frac{\mathrm{d}^2 I_\mathrm{e}}{\mathrm{d}\,V^2} = \frac{e^3 S}{2\sqrt{2m_\mathrm{e}}} \frac{f\left[e(V_\mathrm{p}-V)\right]}{\sqrt{e(V_\mathrm{p}-V)}} = \frac{e^3 S}{2\sqrt{2m_\mathrm{e}}} g\left[e(V_\mathrm{p}-V)\right], \tag{1}$$

wherein e is the elementary charge, S the probe collection area, m_e the electron mass, V_p the plasma potential and V the probe potential. The quantity $g(\varepsilon)$ is frequently referred to as the electron energy probability function. It is expressed in $\mathrm{m}^{-3}\,\mathrm{J}^{-3/2}$, whereas the unit of the EEDF is $\mathrm{m}^{-3}\,\mathrm{J}^{-1}$. For an isotropic plasma, the EEDF and the EEPF contain an identical amount of information. Note that the probe potential is below the plasma potential: $V < V_\mathrm{p}$. In fact, the probe acts as an electron energy filter in the electron-retarding region. The value of the plasma potential is thereby the proper zero of the energy scale of the EEDF. The second derivative of the $I(V)$ trace necessary for the estimation of the EEDF can be either measured directly (online methods [18]) or numerically computed from the experimental data (offline methods). In the present work, the second derivative of the probe I–V characteristic curve was obtained by numerical differentiation using the *Start* program developed by Pavel Kudrna at the Charles University in Prague. For convenience the EEDF, as well as the EEPF, is normalized to the electron density n_e in the program. Figure 4 shows in a semi-log scale an EEDF. The associated EEPF is also plotted. The measurements have been performed on the thruster centerline at $x = 250$ mm. The EEPF is fairly a straight line in this graph, which means the electron distribution function is close to Maxwellian. The time scale used in this study is illustrated in figure 5. The time origin $t = 0$ is set arbitrarily at the maximum of the harmonic voltage applied to the keeper electrode.

The electron density n_e, as well as the electron temperature T_e, can be obtained from the EEDF or the EEPF. Contrary to the standard Langmuir probe theory, this approach is valid for any arbitrary EEDF shape. In other words, it does not

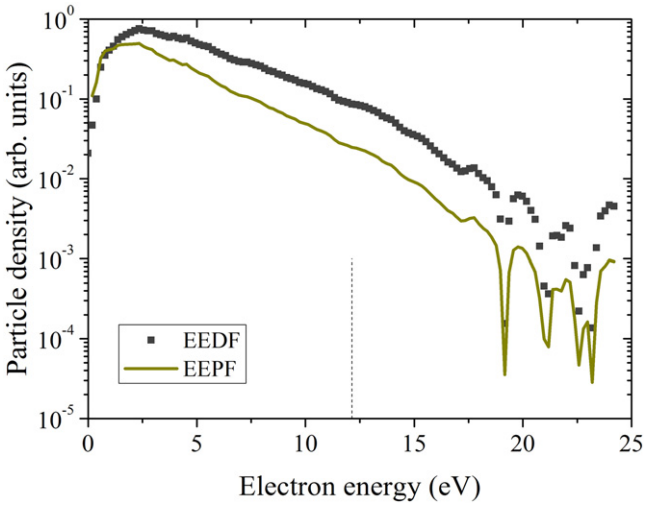

Figure 4. EEDF and corresponding EEPF measured on the thruster axis 250 mm downstream from the channel exit plane ($t = 0\,\mu$s; see figure 1). The noise level of the EEPF was assessed to be around 10^{-4}. The dashed line indicates the xenon ionization potential.

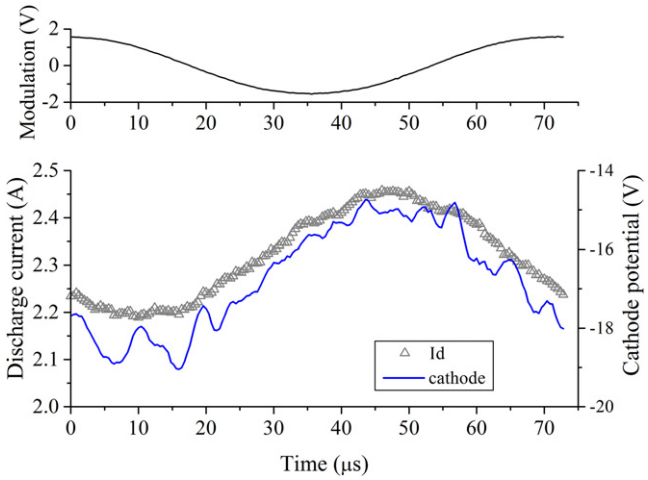

Figure 5. Anode discharge current trace (triangle) and cathode potential trace (line) during one breathing oscillation period. Also shown is the modulation signal. The time scale is the one used for all datasets.

require the assumption of an equilibrium Maxwellian EEDF. The electron density is found by integrating the EEDF over all possible energies:

$$n_e = \int_0^\infty f(\varepsilon)\mathrm{d}\varepsilon = \int_0^\infty \sqrt{\varepsilon} g(\varepsilon)\mathrm{d}\varepsilon. \quad (2)$$

The average electron kinetic energy $\langle\varepsilon\rangle$ is given by the first-order moment of the EEDF. An effective electron temperature can be defined from $\langle\varepsilon\rangle$. The following expressions hold:

$$\langle\varepsilon\rangle = \frac{1}{n_e}\int_0^\infty \varepsilon\, f\,(\varepsilon)\ \mathrm{d}\varepsilon \quad (3)$$

and

$$T_e = \frac{2}{3} k_B \langle\varepsilon\rangle\,, \quad (4)$$

wherein k_B is Boltzmann's constant. Equations (2) and (4) give $n_e = 10^{16}\,\mathrm{m}^{-3}$ and $T_e = 4.3\,\mathrm{eV}$, respectively, for the EEDF displayed in figure 4 ($x = 250\,\mathrm{mm}$ and $t = 0\,\mu$s). In the remainder of the paper, n_e and T_e are determined using previous equations unless specified otherwise. The uncertainty associated with these two quantities is around 20% due to the I–V curve measurement error bar combined with the computation of the second derivative.

4. Results and discussion

4.1. Time evolution of the EEDF

The evolution in time of the anode discharge current and of the cathode potential versus ground during acquisition of the Langmuir probe I–V curve is shown in figure 5. The two traces are a temporal average over 30 periods. Also shown is the modulation signal applied to the keeper electrode. In figure 5, the span of time corresponds to one breathing oscillation. The time scale, especially the origin, is similar for all datasets. The starting point ($t = 0$) is defined arbitrarily at the maximum amplitude of the modulation waveform. As can be seen in figure 5, the discharge current waveform and cathode potential waveform are in phase.

Figure 6 shows the evolution in time of the EEPF measured at four positions in the plume far-field. The position $x = 0\,\mathrm{mm}$ and $y = 0\,\mathrm{mm}$ corresponds, respectively, to the channel exit plane and the thruster centerline. As can be seen in figure 6, the EEPF does not vary very much in the course of time, whatever the location in the plasma plume. Changes, both in amplitude and shape, are relatively small; however, measurements indicate the EEDF does oscillate at the breathing frequency. Note that a large fraction of the electron population has a kinetic energy below 10 eV. This is not surprising as the plume is an expanding recombining plasma [14]. In fact, the EEDF is Maxwellian. This is better seen in figure 7. The EEPF is linear until the energy reaches the Xe atom first ionization energy (12.1 eV). The tail of the EEPF is seemingly depleted above the ionization energy. Plots indicate the depletion is more pronounced far away from the exit plane in the sense that the energy threshold shifts toward a lower value. For instance, the EEPF is an undisturbed Maxwellian at $x = 250\,\mathrm{mm}$. At a large angle (large y), the EEPF seems to be depleted for an energy below the ionization energy. The signal-to-noise ratio is, however, in the order of the statistical noise at high energy and additional data is necessary to validate this fact.

4.2. Electron density and temperature

As explained in section 3, both the electron density and the electron temperature can be inferred from the EEDF—see equation (2) and equation (4). The evolution in time of the electron density n_e is displayed in figure 8. The time-series corresponds to EEDF(t) measurements carried out 250 mm downstream of the thruster exit plane on the thruster axis ($y = 0$). The density oscillates at 13.8 kHz with a ≈10% change in magnitude, above our measurement accuracy, which is 2%. The change in density is relatively low compared to other works [11]. It, however, certainly depends on the thruster design and on the operation regime. Note that here the fluctuation level of n_e and I_d are in the same order of

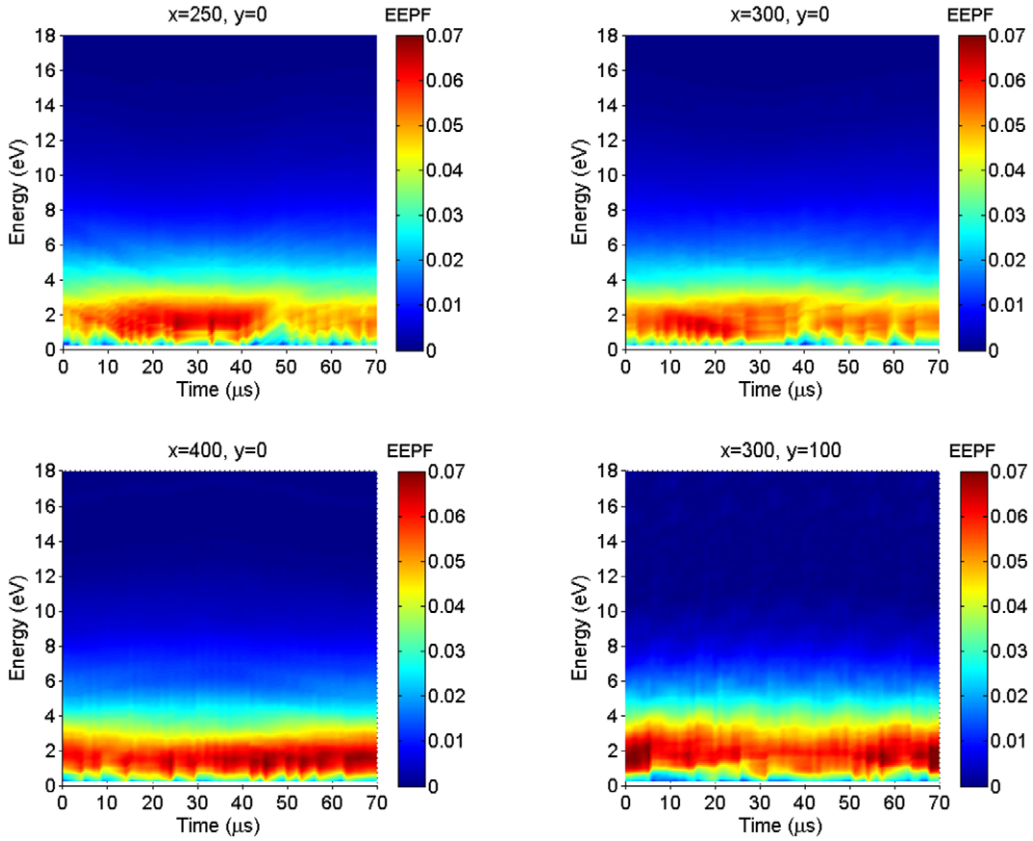

Figure 6. The evolution in time of the EEPF for four positions in the plume during one breathing oscillation period. The EEPF are normalized to the electron density and expressed in $eV^{-3/2}$.

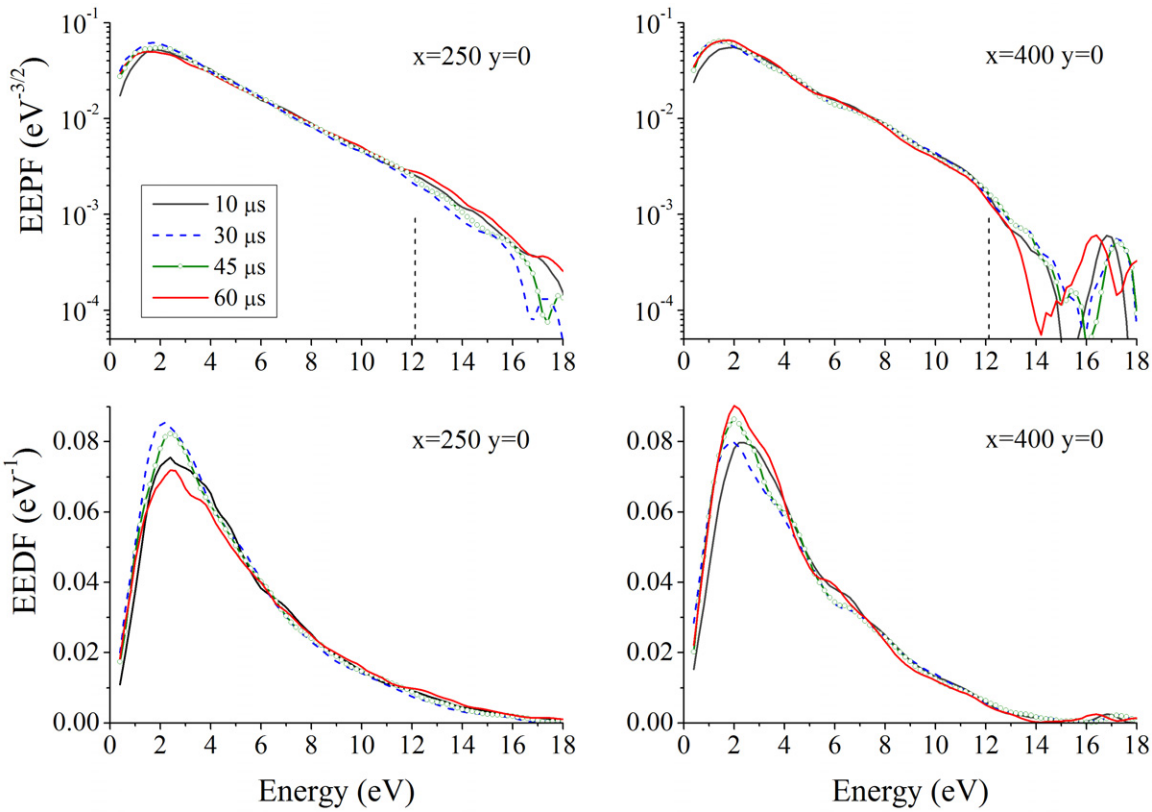

Figure 7. The EEPF and EEDF at successive moments during one breathing oscillation period for two positions. Distributions are normalized to the electron density. The dashed line indicates the ionization energy for the xenon atom.

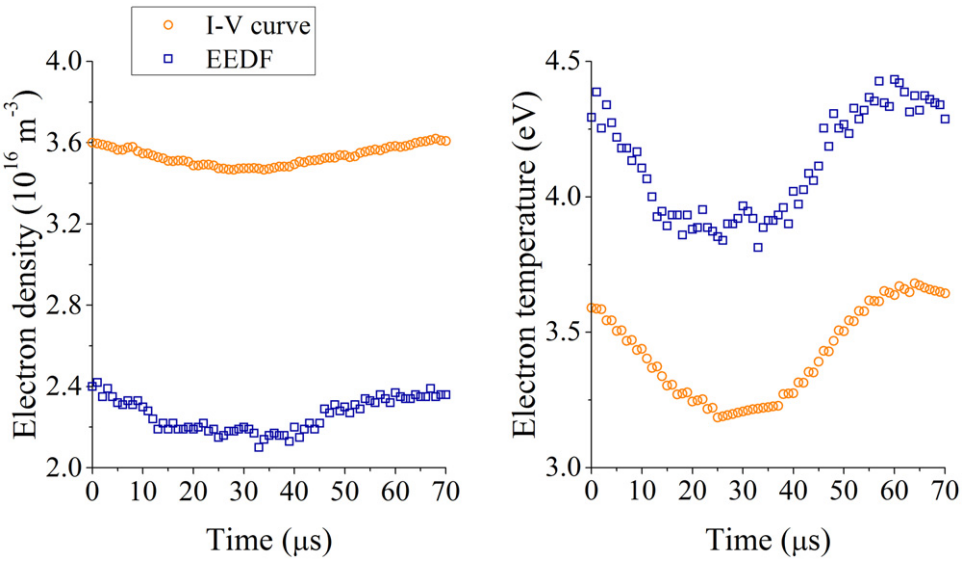

Figure 8. Time evolution of n_e (left) and T_e (right) at $x = 250$ mm and $y = 0$: from the I–V characteristic (circle) and from the EEDF (square).

magnitude. One can plot the time evolution of the electron temperature computed from the EEDF. The result is shown is figure 8. The temperature also oscillates at the breathing mode frequency with about 10% of amplitude change. Note that T_e is minimum when n_e is minimum at this position. The electron parameters can also be obtained from the probe I–V characteristic curve assuming a Maxwellian electron distribution function [19]. The electron temperature was determined from the slope of the logarithm of the electron current in the transition region. The electron density was calculated using the orbital motion limited (OML) assumption; the slope of the I_e^2 against V plot is proportional to n_e^2. Results are displayed in figure 8 for comparison. In this case, the temporal behavior of the two quantities does not depend on the method. It is due to the fact that the EEDF does not depart much from a Maxwellian function. However, there is a difference in amplitude. The temperature is somewhat lower and the density somewhat higher when using the I–V curve. The difference remains in the error margin associated with the data extraction process, which can exceed 20% because of the numerical calculation of the EEDF and the theory behind analysis of the I–V curve.

Figure 9 presents the electron density and temperature time series during one breathing period for three positions along the thruster centerline. As can be seen, both n_e and T_e decrease when moving downstream. The plasma plume of an HT is an isentropic expansion, as shown in a preceding work [14]. More interesting is the fact that there is a space-dependent phase-shift, which is clearly seen in the temperature graph. Besides, the phase difference between n_e and T_e seems to increase with the position x along the axis, although the error bar is large for $x = 300$ and 400 mm. A space-dependent phase indicates that the discharge does not oscillate as a bulk. In other words, the breathing oscillation propagates in the plasma plume toward the outside. Such a phenomenon has previously been observed and succinctly described by Lobbia [11]. A propagation velocity v can be inferred from our dataset. Assuming a constant velocity between $x = 250$ mm and $x = 400$ mm, one finds $v = (2700 \pm 700)\,\mathrm{m\,s^{-1}}$ using n_e and T_e time series. This value is well above the neutral gas speed ($\approx$200 m s^{-1}) measured by laser spectroscopy in the plume near the field [20]. But it is close to the ion acoustic speed v_s. The latter reads [21]:

$$v_s = \sqrt{\frac{Zk_B T_e + 3k_B T_i}{m}}, \tag{5}$$

wherein Z is the ion charge, T_i is the ion temperature and m is the ion mass. When solely considering singly charged Xe^+ ion species ($Z = 1$), the acoustic speed is 2300 m s^{-1} with $T_e = 4$ eV and $T_i = 1$ eV. Note that T_i cannot be neglected compared to T_e in a Hall thruster discharge [22]. Our EEDF(t) measurements therefore suggest there is a wave at the breathing frequency traveling in the plasma with the ion acoustic velocity. Longitudinal propagation of plasma disturbances with the ion acoustic speed in a Hall thruster discharge has recently been highlighted by means of collective Thomson scattering on the electron fluid [23].

5. Conclusion

Time-resolved Langmuir probe measurements performed in the plume of the 1.5 kW-class PPS®1350-ML Hall thruster allowed us to compute the time-varying EEDF. The distribution function changes periodically in the course of time. As expected, the period corresponds to the breathing oscillation. The EEDF is Maxwellian with a depleted tail above the xenon ionization energy whatever the location and the time. The electron density and temperature have been computed from the EEDF. The two quantities oscillate at the breathing mode frequency. Our data analysis seems to confirm the existence of a low-frequency plasma wave, which has been previously observed by probes on a different thruster and on the same thruster by coherent Thomson scattering. The

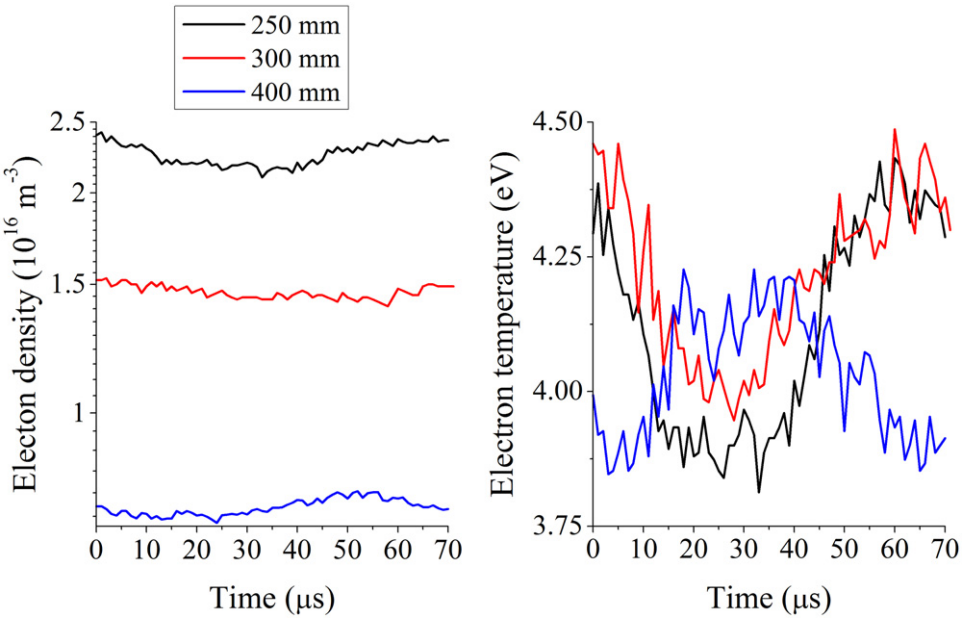

Figure 9. Time evolution of n_e (left) and T_e (right) for various positions along the thruster axis ($y = 0$). Traces show a space-dependent phase-shift.

wave front propagates axially with a speed compatible with the ion acoustic speed. However, other measurement series are necessary to get more information about the plasma wave propagation. For instance, the time-dependent EEDF must be captured for various thruster operating conditions. In addition, probe measurements must be carried out in the vicinity of the channel exit plane.

Acknowledgments

This work was carried out in the framework of the CNRS/CNES/SNECMA/Universités joint research program GdR 3161 entitled 'Propulsion par plasma dans l'espace'. M Tichý and P Kudrna acknowledge financial support by the CNES and by the Czech Science Foundation under the grant P205/11/0386.

References

[1] Goebel D M and Katz I 2008 *Fundamentals of Electric Propulsion* (Hoboken, NJ: Wiley)
[2] Frisbee R H 2003 Advanced space propulsion for the 21st century *J. Propul. Power* **19** 1129
[3] Choueiri E Y 2009 New dawn for electric rockets *Sci. Am.* **300** 58
[4] Zhurin V V, Kaufmann H R and Robinson R S 1999 Physics of closed drift thrusters *Plasma Sources Sci. Technol.* **8** R1
[5] Dannenmayer K and Mazouffre S 2011 Elementary scaling relations for Hall effect thrusters *J. Propul. Power* **27** 236
[6] Esipchuck Y B, Morozov A I, Tilinin G N and Trofimov A V 1974 Plasma oscillations in closed-drift accelerators with an extended acceleration zone *Sov. Phys.—Tech. Phys.* **18** 928
[7] Choueri E Y 2001 Plasma oscillations in Hall thrusters *Phys. Plasmas* **8** 1411
[8] Boeuf J P and Garrigues L 1998 Low frequency oscillations in a stationary plasma thruster *J. Appl. Phys.* **84** 3541
[9] Barral S and Peradzyński Z 2010 Ionization oscillations in Hall accelerators *Phys. Plasmas* **17** 014505
[10] Smith A W and Cappelli M A 2009 Time and space-correlated plasma potential measurements in the near field of a coaxial Hall plasma discharge *Phys. Plasmas* **16** 073504
[11] Lobbia R B and Gallimore A D 2008 A method of measuring transient plume properties *Proc. 44th Joint Propulsion Conf. (Hartford, CT)* AIAA paper 2008-4650
[12] Dannenmayer K, Kudrna P, Tichý M and Mazouffre S 2012 Time-resolved measurement of plasma parameters in the far-field plume of a low-power Hall effect thruster *Plasma Sources Sci. Technol.* **21** 055020
[13] Koppel C R and Estublier D 2005 The SMART-1 Hall effect thruster around the moon: In flight experience *Proc. 29th Int. Electric Propulsion Conf. (Princeton, NJ)* paper 2005-119
[14] Dannenmayer K and Mazouffre S 2013 Electron flow properties in the far-field plume of a Hall thruster *Plasma Sources Sci. Technol.* **22** 035004
[15] Vaudolon J, Balika L and Mazouffre S 2013 Photon counting technique applied to time-resolved laser-induced fluorescence measurements on a stabilized discharge *Rev. Sci. Instrum.* **84** 073512
[16] Demidov V I, Ratynskaia S V and Rypdal K 2002 Electric probes for plasmas: The link between theory and instrument *Rev. Sci. Instrum.* **73** 3409–39
[17] Godyak V A and Demidov V I 2011 Probe measurements of electron-energy distributions in plasmas: what can we measure and how can we achieve reliable results? *J. Phys. D: Appl. Phys.* **44** 233001
[18] Luijendijk S C M and Van Eck J 1967 Comparison of three devices for measuring the second derivative of a Langmuir probe curve *Physica* **36** 49
[19] Chung P M, Talbot L and Touryan K J 1975 *Electric Probes in Stationary and Flowing Plasmas: Theory and Application* (New York: Springer)
[20] Mazouffre S, Bourgeois G, Garrigues L and Pawelec E 2011 A comprehensive study on the atom flow in the cross-field discharge of a Hall thruster *J. Phys. D: Appl. Physics* **44** 105203
[21] Chen F F 1984 *Introduction to Plasma Physics and Controlled Fusion* vol 1 (New York: Plenum) p 96

Goebel D M and Katz I 2008 *Fundamentals of Electric Propulsion* (Hoboken, NJ: Wiley)

[22] Mazouffre S 2013 Laser-induced fluorescence diagnostics of the cross-field discharge of Hall thrusters *Plasma Sources Sci. Technol.* **22** 013001

[23] Tsikata S, Honoré C, Grésillon D, Héron A, Lemoine N and Cavalier J 2011 Observation of ion beam properties in the Hall thruster plasma using an axial electron density fluctuation mode *Proc. 32nd Int. Electric Propulsion Conf. (Wiesbaden, Germany)* paper 2011-225